Chemical Engineering Science 65 (2010) 3260–3267

Contents lists available at ScienceDirect

Chemical Engineering Science

journal homepage: www.elsevier.com/locate/ces

Numerical simulation of non-isothermal pressure-driven miscible channel flow with viscous heating

K.C. Sahu [a,*], H. Ding [b], O.K. Matar [c]

[a] Department of Chemical Engineering, Indian Institute of Technology, Hyderabad, India
[b] Department of Chemical Engineering, University of California, Santa Barbara, USA
[c] Department of Chemical Engineering, Imperial College London, UK

ARTICLE INFO

Article history:
Received 13 October 2009
Received in revised form
31 January 2010
Accepted 6 February 2010
Available online 11 February 2010

Keywords:
Isothermal flow
Viscous heating
Channel flow
Miscible flow
Stability
Interfacial flow

ABSTRACT

We study the pressure-driven, non-isothermal miscible displacement of one fluid by another in a horizontal channel with viscous heating. We solve the continuity, Navier–Stokes, and energy conservation equations coupled to a convective-diffusion equation for the concentration of the more viscous fluid. The viscosity is assumed to depend on the concentration as well as the temperature, while density contrasts are neglected. Our transient numerical simulations demonstrate the development of 'roll-up' of the 'interface' separating the fluids and vortical structures whose intensity increases with the temperature of the invading fluid. This brings about fluid mixing and accelerates the displacement of the fluid originally occupying the channel. Increasing the level of viscous heating gives rise to high-temperature, low-viscosity near-wall regions. The increase in viscous heating retards the propagation of the invading fluid but accelerates the ultimate displacement of the resident fluid.

1. Introduction

The dynamics of two-fluid flows has been the subject of numerous experimental, theoretical and numerical studies due to their central importance to a number of applications; these range from the transportation of crude oil in pipelines (Joseph et al., 1997), mixing of liquids using, for instance, static mixers (Cao et al., 2003), and the cleaning of plants, which involves removal of viscous fluids by fast-flowing water streams (Regner et al., 2007). In the latter case, achieving fundamental understanding of these flows permits the determination of the degree of mixing between the fluids and minimization of the amount of waste-water utilized.

The stability of immiscible fluids (Yih, 1967; Hickox, 1971; Joseph et al., 1984, 1997; Hu and Joseph, 1989; Joseph and Renardy, 1992; Kouris and Tsamopoulos, 2001b, 2002b) has received the majority of the attention in the literature. The studies involving the flow of such fluids have examined their linear stability in planar channels in the long-wave limit (Yih, 1967) and for short waves (Hooper and Boyd, 1983; Hinch, 1984; Yiantsios and Higgins, 1988); this work has been reviewed by Boomkamp and Miesen (1996). The linear stability of immiscible core-annular flows has also been studied (Joseph and Renardy, 1992; Joseph et al., 1997) in horizontal (Joseph et al., 1984; Renardy and Joseph, 1985; Hu and Joseph, 1989; Preziosi et al., 1989; Hu et al., 1990) and vertical pipes (Hickox, 1971; Hu and Patankar, 1995); this work has been complemented by experimental (Charles et al., 1961; Bai et al., 1992) and numerical investigations in both corrugated (Kouris and Tsamopoulos, 2001a, 2002a; Wei and Rumschitzki, 2002a, 2002b) and smooth (Li and Renardy, 1999; Kouris and Tsamopoulos, 2001b, 2002b) pipes.

In contrast, the stability of miscible two-fluid flows has received less attention. The linear stability work of Ranganathan and Govindarajan (2001) and Govindarajan (2004) has demonstrated that three-layer Poiseuille flow is unstable at high Schmidt numbers and low Reynolds numbers; while that of Ern et al. (2003) has shown that for rapidly varying viscous stratification, diffusion can be destabilizing. Experimental work on core-annular miscible flows has focused on determining the thickness of the wall layer, following the displacement of a highly viscous fluid by a less viscous one, and the tip speed of the propagating 'finger' of the latter (Taylor, 1961; Cox, 1962; Petitjeans and Maxworthy, 1996; Chen and Meiburg, 1996; Kuang et al., 2003; Balasubramaniam et al., 2005). The developments of axisymmetric and 'corkscrew' patterns have also been investigated (Lajeunesse et al., 1997, 1999; Scoffoni et al., 2001; Gabard and Hulin, 2003; Cao et al., 2003) as has the formation of 'pearls' and 'mushrooms' in the case of neutrally buoyant, miscible core-annular flows in

* Corresponding author.
E-mail address: ksahu@iith.ac.in (K.C. Sahu).

0009-2509/$ - see front matter © 2010 Elsevier Ltd. All rights reserved.
doi:10.1016/j.ces.2010.02.017

horizontal pipes at high Schmidt number and Reynolds numbers in the range 2–60 (d'Olce et al., 2008); the latter work has demonstrated that the transition from 'pearls' to 'mushrooms' occurs with increasing Reynolds number and/or core radius, for a fixed viscosity ratios.

The recent and comprehensive work of Selvam et al. (2007) on the linear stability of neutrally buoyant, core-annular flows has shown that, above a critical viscosity ratio, the flow is unstable even when the less viscous fluid is at the wall. This is in contrast to the case of immiscible, lubricated pipelining (Joseph et al., 1997) and to miscible channel flows (Malik and Hooper, 2005): these flows are stable in this configuration (although it should be noted that the range of parameters over which this is true is limited). This study also shows that at relatively small Reynolds numbers, large Schmidt numbers and wavenumbers, axisymmetric (corkscrew) modes are dominant if the more (less) viscous fluid is in the pipe core. The stability of neutrally buoyant, two-fluid miscible channel flows was also examined recently by Sahu et al. (2009a) for large viscosity contrasts. They solved the Navier–Stokes equations coupled to a convective-diffusion equation for the concentration of the more viscous fluid. For the case of a three-layer flow, with the more viscous fluid at the walls, they carried out a generalized spatio-temporal linear stability analysis (Huerre and Monkewitz, 1990; Chomaz, 2005; Schmid and Henningson, 2001) and determined the boundaries between convectively and absolutely unstable flows in the space of the Reynolds number and viscosity ratio, for parameterically varying Schmidt numbers. This analysis identified the vertical gradients of viscosity perturbations as the main destabilizing influence (see also Selvam et al., 2007). Their transient numerical simulations of the flow in the nonlinear regime, demonstrated the development of complex dynamics; these are characterized by 'roll-up' and convective mixing, which increase in intensity with increasing viscosity ratio, Reynolds and Schmidt numbers. A similar analysis to study the convective and absolute nature of instabilities in miscible core annular flows at high Schmidt numbers was also conducted by Selvam et al. (2009). This system was also studied experimentally by d'Olce et al. (2009). They observed absolute instabilities for a range of core radii for high viscosity ratios when the less viscous fluid is in the core.

The work of Sahu et al. (2009a) has been extended to account for buoyancy effects in inclined channels via numerical solution of the Navier–Stokes equations, without the Boussinesq approximation, coupled to a convective-diffusion equation for the concentration of the more viscous fluid through a concentration-dependent viscosity and density (Sahu et al., 2009b). The effect of density ratio, Froude number, and channel inclination was investigated. Their results demonstrated that the rates of mixing and displacement of the more viscous fluid are promoted by the development of Rayleigh–Taylor instabilities, and enhanced with increasing density ratio and Froude number. The mixing rates were also shown to increase with increasing inclination angles when the displaced fluid is also the denser one.

As the above brief review shows, the work carried out on two-fluid miscible channel flows has so far been for isothermal systems only. Yet, thermal gradients can potentially have a drastic effect on the flow dynamics due to their influence on the density and viscosity. In the present work, we extend the work of Sahu et al. (2009a) and investigate the effect of temperature variations on the nonlinear dynamics of the flow for horizontal channels and neutrally buoyant systems. We solve the continuity, Navier–Stokes and energy conservation equations coupled to a convective-diffusion of the concentration of the more viscous fluid. The viscosity is taken to be a function of this concentration as well as the temperature in the channel, while the thermal conductivity is assumed to be a function of the concentration only. We elucidate, through transient numerical simulations, the effect of initial temperature differences between the displacing fluid and that already present in the channel, as well as viscous heating on the flow dynamics.

The rest of this paper is organized as follows. The problem is formulated in Section 2, and the results of the numerical simulations are presented in Section 3. Concluding remarks are provided in Section 4.

2. Problem formulation

2.1. Governing equations and non-dimensionalization

We consider the two-dimensional miscible channel flow, wherein a stationary, Newtonian and incompressible fluid, initially occupying the channel completely, is displaced by a less viscous fluid. The temperatures of the fluid occupying the channel initially and the inlet fluid are T_1 and T_2, respectively, and the channel walls are maintained at temperature T_1, as shown in Fig. 1. We assume that the densities of both the fluids are the same and use a rectangular coordinate system, (x,y), to model the flow dynamics, where x and y denote the horizontal and vertical coordinates, respectively. The channel inlet and outlet are located at $x=0$ and L, and its walls, which are rigid and impermeable, are located at $y=0$ and H, respectively.

The following Nahme-type functional dependence (Nahme, 1940; Sukanek et al., 1973; Pinarbasi and Ozalp, 2001; Sahu and Matar, 2010) is used for the viscosity:

$$\mu = \mu_2(T_1) e^{[\ln\, m - \beta((T-T_1)/T_1)]}, \tag{1}$$

where β is a dimensionless activation energy parameter, which characterizes the sensitivity of the viscosity to the temperature variation; for liquids, β is a positive number, and we restrict ourselves to this case; c is the concentration, which represents the fraction of the channel occupied by the more viscous fluid at a reference temperature T_1; $m(\equiv \mu_1(T_1)/\mu_2(T_1))$ is the viscosity ratio, wherein $\mu_1(T_1)$ and $\mu_2(T_1)$ are the viscosities of the fluid occupying the channel and the inlet fluid at T_1, respectively.

The following scaling is employed in order to render the governing equations dimensionless:

$$\begin{aligned} &(x,y) = H(\tilde{x},\tilde{y}), \quad t = \frac{H}{U_m}\tilde{t}, \quad (u,v) = U_m(\tilde{u},\tilde{v}),\\ &p = \rho U_m^2 \tilde{p}, \quad T = \frac{T_1\tilde{T}}{\beta} + T_1,\\ &\mu = \tilde{\mu}\mu_2, \quad \kappa = \tilde{\kappa}\kappa_2, \end{aligned} \tag{2}$$

here the tildes designate dimensionless quantities; $\mathbf{u}=(u,v)$ represents the two-dimensional velocity field where u and v denote the horizontal and vertical velocity components, respectively; $U_m \equiv Q/H$, is the characteristic velocity, where Q is the volumetric flow rate; T, p, ρ and t denote the temperature, pressure, density of the fluid and time, respectively. The viscosity μ and thermal conductivity κ have been scaled on those of the inlet fluid, $\mu_2(T_1)$ and κ_2, at temperature T_1, respectively.

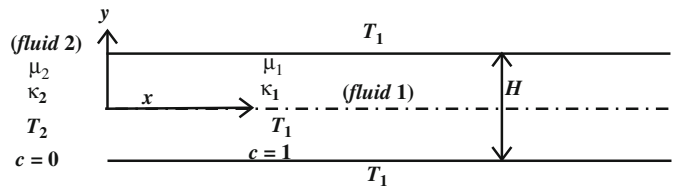

Fig. 1. Schematic diagram of the channel.

After dropping tildes from all non-dimensional terms, the governing equations are given by

$$\frac{\partial u}{\partial x}+\frac{\partial v}{\partial y}=0, \tag{3}$$

$$\frac{\partial u}{\partial t}+u\frac{\partial u}{\partial x}+v\frac{\partial u}{\partial y}=-\frac{\partial p}{\partial x}+\frac{1}{Re}\left[\frac{\partial}{\partial x}\left\{2\mu\frac{\partial u}{\partial x}\right\}+\frac{\partial}{\partial y}\left\{\mu\left(\frac{\partial u}{\partial y}+\frac{\partial v}{\partial x}\right)\right\}\right], \tag{4}$$

$$\frac{\partial v}{\partial t}+u\frac{\partial v}{\partial x}+v\frac{\partial v}{\partial y}=-\frac{\partial p}{\partial y}+\frac{1}{Re}\left[\frac{\partial}{\partial x}\left\{\mu\left(\frac{\partial u}{\partial y}+\frac{\partial v}{\partial x}\right)\right\}+\frac{\partial}{\partial y}\left\{2\mu\frac{\partial v}{\partial y}\right\}\right], \tag{5}$$

$$\frac{\partial c}{\partial t}+u\frac{\partial c}{\partial x}+v\frac{\partial c}{\partial y}=\frac{1}{Re\,Sc}\left(\frac{\partial^2 c}{\partial x^2}+\frac{\partial c}{\partial y^2}\right), \tag{6}$$

$$\frac{\partial T}{\partial t}+u\frac{\partial T}{\partial x}+v\frac{\partial T}{\partial y}=\frac{Na}{Re\,Pr}\mu\left[2\left\{\left(\frac{\partial u}{\partial x}\right)^2+\left(\frac{\partial v}{\partial y}\right)^2\right\}+\left(\frac{\partial u}{\partial y}+\frac{\partial v}{\partial x}\right)^2\right]+\frac{1}{Re\,Pr}\left[\frac{\partial}{\partial x}\left(\kappa\frac{\partial T}{\partial x}\right)+\frac{\partial}{\partial y}\left(\kappa\frac{\partial T}{\partial y}\right)\right] \tag{7}$$

where $Na(\equiv\beta\mu_2(T_1)U_m^2/\kappa_2 T_1)$, $Re(\equiv\rho U_m H/\mu_2)$, $Pr(\equiv c_p\mu_2(T_1)/\kappa_2)$ and $Sc(\equiv\mu_2(T_1)/\mathcal{D}\rho)$ are the Nahme, Reynolds, Prandtl and Schmidt numbers, respectively, wherein $\mathcal{D}$ denotes a constant diffusion coefficient. The dimensionless form of viscosity model is given by

$$\mu=e^{[c\ln m-T]}. \tag{8}$$

We also assume that the dimensionless thermal conductivity has the following dependence on c:

$$\kappa=c(r_\kappa-1)+1, \tag{9}$$

where $r_\kappa\equiv\kappa_1/\kappa_2$ is the thermal conductivity ratio.

In order to determine the flow characteristics, we solve the above continuity and Navier–Stokes equations, coupled to a convection–diffusion equation for the concentration c, and the energy equation subject to the following boundary condition. No-slip and no-penetration conditions are imposed on the velocity vector, and no-flux condition is applied on c at both walls. The channel walls are assumed to be highly conducting so that a condition of T=0 is imposed at y=(0,1). A fully developed velocity profile with a constant flow rate at the inlet (x=0), and Neumann boundary conditions on the velocity at the outlet (x=L) are imposed, where L is the non-dimensional length of the channel. The temperature at the inlet is $r_T(\equiv\beta(T_2-T_1)/T_1)$, and a Neumann boundary condition is also used for the temperature at the outlet (x=L). In the present study, the aspect ratio of the channel is 1:40, and we have ascertained that the results are insensitive to the channel length by ensuring that the aspect ratio is sufficiently large.

2.2. Numerical procedure

In this section, we briefly describe the numerical procedure to solve Eqs. (3)–(7). A staggered grid is used for the finite-volume discretization of these equations, with the scalar variables, the pressure, temperature and concentration, defined at the centre of each cell while the velocity components are defined at the cell faces. The solution methodology employs the following procedure: the concentration and temperature fields are first updated by solving Eqs. (6) and (7), respectively, with the velocity field at time steps n and $n-1$; this is then updated to time-step n+1 by solving Eqs. (4) and (5) together with the continuity equation, Eq. (3). For the spatial discretization, the advective term, the second and third terms on the left-hand-side of Eqs. (6) and (7), are approximated using a weighted essentially non-oscillatory (WENO) scheme, while a central difference schemes is used to discretize the diffusive term on the right-hand-side of Eqs. (6) and (7). A central difference scheme is also used to discretize the viscous heating term, the first term on the right-hand-side of Eq. (7). In order to achieve second-order accuracy in the temporal discretization, the Adams–Bashforth and Crank–Nicolson methods are used for the advective and second-order dissipation terms, respectively, in Eqs. (4) and (5).

The numerical procedure described above has previously been employed by Ding et al. (2007) to solve Eqs. (3)–(5) along with a Cahn–Hilliard equation for the interfacial position within the framework of the 'diffuse interface' method. Sahu et al. (2009a, 2009b) have also used this procedure to simulate the pressure-driven neutrally buoyant, miscible channel flows with high viscosity contrasts. The result of the present paper are discussed next.

3. Results and discussion

In order to inspire confidence in the predictions of the numerical procedure, we have carried out mesh refinement tests by plotting the temporal evolution of a dimensionless measure of the mass of the displaced fluid '1', $M^{0.95}/M_0$, and the position of the leading 'front' separating the two fluids, $x_{\rm tip}$, as shown in Figs. 2a and b, respectively. Here, $M_{0.95}$ and M_0 denote the mass of fluid with $c\geq 0.95$ and that of fluid '1' initially occupying the channel, respectively. The parameter values chosen are Re=400,

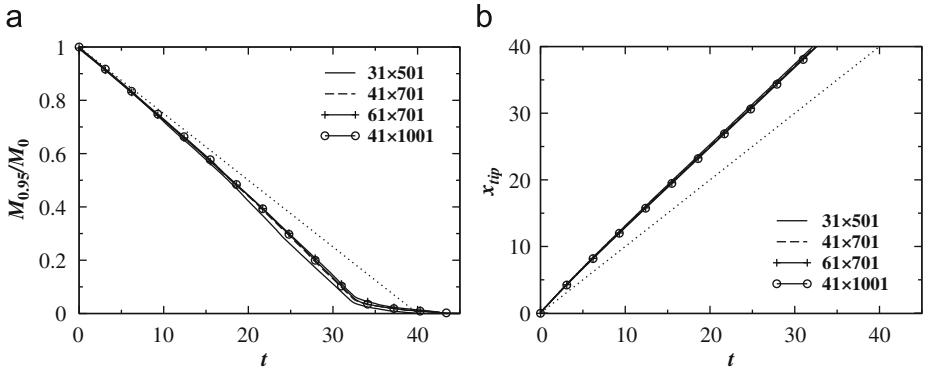

Fig. 2. Mass fraction of the displaced fluid $M_{0.95}/M_0$, (a), and temporal evolution of the position of the leading 'front' separating the two fluids, $x_{\rm tip}$, (b), obtained using different mesh densities for Re=400, Sc=50, Pr=7, Na=5, m=10, $r_\kappa=1$ and r_T=0.5. The dotted lines in panel (a) and (b) represent the limiting case given by $M_{0.95}/M_0=1-tH/L$ and x=t, respectively. This corresponds to the case wherein fluid '1' is displaced by fluid '2' in plug flow and prior to the sharp, vertical interface separating the two fluids exiting the channel.

Sc=50, Pr=7, Na=5, m=10, $r_\kappa = 1$ and r_T=0.5, which are characteristic of a situation where a cold fluid is displaced by a hot fluid.

Inspection of Fig. 2a reveals that the mass fraction of the displaced cold and more viscous fluid decreases from unity, essentially linearly at relatively early times; this occurs between $t \approx 0$ and 32. This early stage of the flow is dominated by the formation of Kelvin–Helmholtz type instabilities. The slope of the curve during this linear stage is considerably steeper than that of the line represented by $1-tH/L$; which corresponds to the plug flow displacement of fluid '1' by fluid '2'. At approximately t=32 for this set of parameters when the 'front' of the displacing fluid '2' reaches the end of simulation domain, a transition to another approximately linear regime occurs. The slope of the $M_{0.95}/M_0$ versus time plot in this regime is much smaller than the previous one, since the flow at this relatively late stage of the dynamics, is dominated by diffusion that acts to mix the fluids on longer time scales. As shown in Fig. 2b, the position of the leading 'front' separating the two fluids, x_{tip}, however, exhibits a linear dependence on time. Inspection of Fig. 2 also reveals that convergence of the results has indeed been achieved upon mesh refinement. The results discussed in the rest of this paper were therefore generated using 41 × 701 grid points, for channels of aspect ratio of 1:40.

We first consider the isothermal case studied by Sahu et al. (2009a). The spatio-temporal evolution of the concentration contours are shown for this case in Fig. 3 with r_T=0 and Na= 0; the rest of the parameter values are Re =500, Sc=100, Pr=7, m=10 and $r_\kappa = 1$. It can be seen in Fig. 3 for t=5 that the 'interface' becomes unstable; instabilities are symmetrical initially. Then these instabilities become asymmetrical forming vortical structures and 'roll-up' of the diffuse 'interface' separating the fluids; this give rise to intense mixing of the two fluids that can be seen for $t \geq 15$ in Fig. 3. This mixing is responsible for the slope of the $M_{0.95}/M_0$ curves being greater than $-H/L$ during the early linear stage for $t \leq 32$ (corresponds to the time when the 'finger' has exited the channel) in Fig. 2a. After this, the remnants of fluid '1' assume the form of thin layers adjacent to the upper and lower walls; the flow is then dominated by diffusion. This change in the character of the flow, from intensely convective to diffusive, is primarily responsible for the change in the slope of the $M_{0.95}/M_0(t)$ plot for $t \geq 32$ in Fig. 2a.

Next, in Fig. 4 we study the effect of r_T, the non-dimensional temperature of fluid '2', on the displacement characteristics in the absence of viscous heating, with the rest of the parameter values remaining unchanged from those used to generate Fig. 3. It can be seen in Fig. 4a that increasing r_T progressively from r_T=0 to 3 leads to more rapid displacement of fluid '1' in comparison to the isothermal case. Similarly, decreasing r_T from r_T=0 decreases the displacement process, which appears to be weakly dependent on the value of r_T for $r_T < 0$. In Fig. 4b, it can be seen that the position of the leading 'front' separating the two fluids, x_{tip}, is very weakly dependent on variations in r_T values. It can also be seen that all the curves in Fig. 4a lie below $1-tH/L$ (and these in Fig. 4b are above $x_{\text{tip}}=t$) which corresponds to 'plug flow' displacements. This is due to the presence of instabilities which enhance mixing and increase the displacement rate.

In Fig. 5, the above results are rationalized by examining the concentration, temperature and viscosity contours for $r_T = -3$ and 3 at t=20. The rest of the parameter values remain unchanged from those used to generate Fig. 3; $r_T = -3$ (r_T=3) corresponds to the case when a cooler (hotter) fluid displaces a hotter (cooler) one. For $r_T = -3$, it can be seen that fluid '1' is penetrated by a relatively stable 'finger' of fluid '2' with a sharp 'nose' separating the two fluids. Similar observations were made by Sahu et al. (2009a) who studied the isothermal case: they observed sharp-nosed finger-formation and found that the onset of 'roll-up' is delayed with decreasing viscosity contrast; this is because viscous stratification is the primary source of instability as identified by these authors and Selvam et al. (2007). In contrast to the $r_T = -3$ case, for r_T=3, the flow appears to be considerably more unstable due to the associated increase in viscosity contrasts. As a result, the region separating fluids '1' and '2' is highly diffuse and hence a higher displacement rate is observed for r_T=3 as compared to $r_T = -3$.

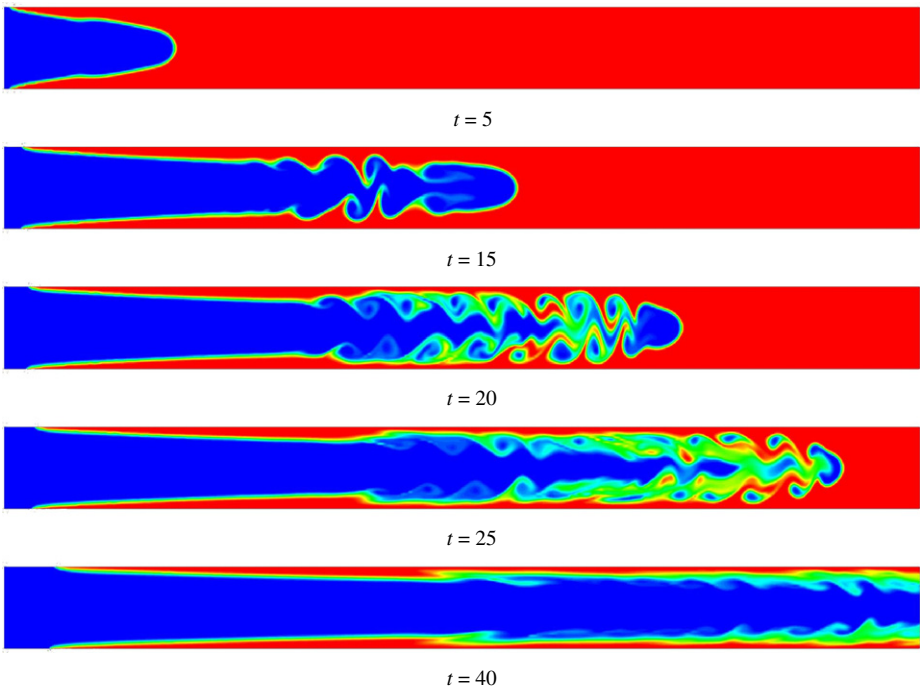

Fig. 3. Spatio-temporal evolution of the concentration contours for the isothermal (r_T=Na= 0). The rest of the parameter values are Re=500, Sc=100, Pr=7, m=10 and $r_\kappa = 1$.

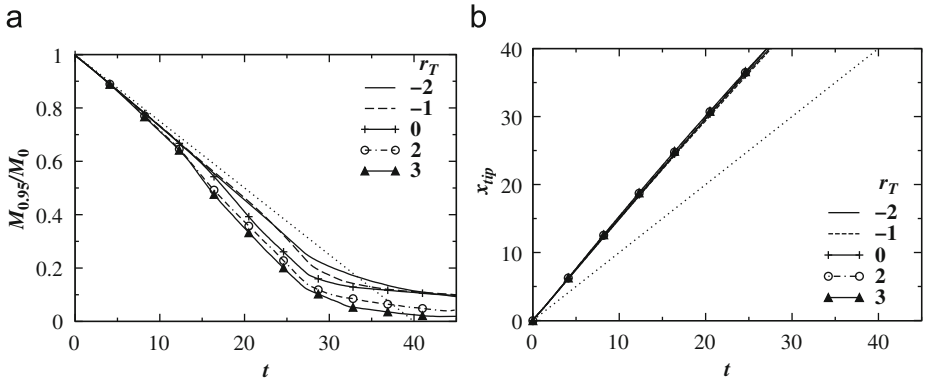

Fig. 4. The effect of r_T on the mass fraction of the displaced fluid '1', (a), the temporal evolution of the position of the leading 'front' separating the two fluids x_{tip}, (b), for $Na=0$. The rest of the parameter values are $Re=500$, $Sc=100$, $Pr=7$, $m=10$ and $r_\kappa=1$. The dotted lines in panels (a) and (b) are the analogues of those shown in Fig. 2 a and b, respectively.

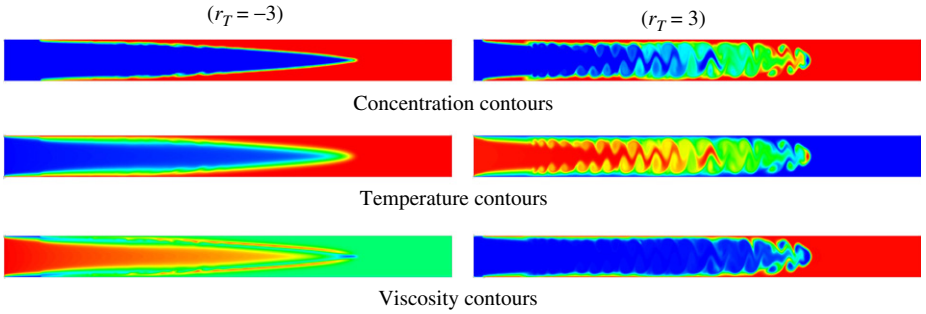

Fig. 5. The concentration, temperature and viscosity contours at $t=20$ for $r_T=-3$ and 3. The rest of the parameter values remain unchanged from those used to generate Fig. 3.

We have also analyzed Fig. 5 by plotting the evolution of the transverse variation of the axially averaged temperature, $\overline{T}_x \equiv (1/L)\int_0^L T\,dx$, and viscosity $\overline{\mu}_x \equiv (1/L)\int_0^L \mu\,dx$ for $r_T=-3$ and $r_T=3$ in Fig. 6(a) and (b), and (c) and (d), respectively. It can be seen in Fig. 6a that $\overline{T}_x$ in the core region decreases with time as the 'finger' of the relatively cool fluid '2' penetrates fluid '1', with relatively warm regions adjacent to the walls. This is accompanied by an increase in the axially averaged viscosity in the core region, as shown in Fig. 6b, which is as expected since the viscosity is a decreasing function of temperature. Close inspection of Fig. 6b also reveals that although the temperature of the channel walls is constant, as the 'finger' of the low concentration fluid '2' penetrates fluid '1', the concentration of this fluid near the walls decreases with time, which is associated with the decrease in the axially averaged viscosity near the wall regions. The increase in the $\overline{\mu}_x$ in the core acts to retard the displacement of fluid '2' in comparison with the isothermal case, as was also observed in Fig. 4 a. For the case of the warmer fluid '1' displacing fluid '2', characterized by $r_T=3$, the reverse is observed: as shown in Fig. 6c and d, $\overline{T}_x$ increases in the core which leads to less viscous region in the core. The values achieved by $\overline{\mu}_x$ throughout the domain for$r_T=-3$ exceed those associated with $r_T=3$ and provide the reason for the smaller displacement rates in the former case.

The effect of varying the degree of viscous heating, characterized by Na, on the dynamics is investigated next. In this case $r_T=1$, and the rest of the parameter values remain unchanged from those used to generate Fig. 3. It can be seen in Fig. 7a and b that increasing Na increases the displacement rate and decreases the velocity of the 'finger' tip, respectively. Since $r_T=1$ in this graph, a hot 'finger' penetrates into a cold fluid, which becomes unstable, rather like a jet, as seen in Fig. 8. This pushes a cooler region in the core of the channel in which the viscosity is relatively high. In this region, the shear rate is very small so viscous heating effects are minimal. At the walls, however, the magnitude of the shear rate is highest as are viscous heating effects. This leads to an increase in the temperature near the walls and a decrease in the viscosity. It is expected, therefore, that the 'finger' penetrate faster for $Na>0$ since it will be 'lubricated' at the walls by low-viscosity regions. Inspection of Fig. 7b, however, demonstrates that this is, in fact, not the case.

This observation can be explained by analyzing Fig. 9, which reveals that there is a change in the character of the temperature and viscosity curves as Na is increased. For $Na=0$, there is clearly a high-temperature, low-viscosity core. The contrast in viscosity between the wall and the core also increases with time. For $Na>0$, at relatively early times, the temperature is higher near the wall regions than in the core; the opposite behaviour can be observed in the viscosity field, as expected, with minima in $\overline{\mu}_x$ corresponding to the near-wall peaks in $\overline{T}_x$. This is quite different from what happens in the $Na=0$ at the same time (e.g. $t=10$). The structure of $\overline{T}_x$ profile then undergoes a change becoming more uniform in the y-direction at late times with a shallow maximum in the core and a corresponding minimum in $\overline{\mu}_x$ (see Fig. 9c and d); this is brought about by heat transfer between the wall and the core regions. This delay in the reduction of $\overline{\mu}_x$ may explain the lower displacement rates associated with increasing Na (see Fig. 7). In the $Na=10$ case, the viscous heating at the walls is so vigorous that the temperature contrast between the core and wall regions is high and persists to late times. As a result, one quickly arrives at a state wherein a high-viscosity fluid is moving in the channel with 'lubricated', low-viscosity near-wall regions. This acts to decelerate the rate of propagation of the 'finger' in the channel. Interestingly, however, the removal rate of fluid '1'

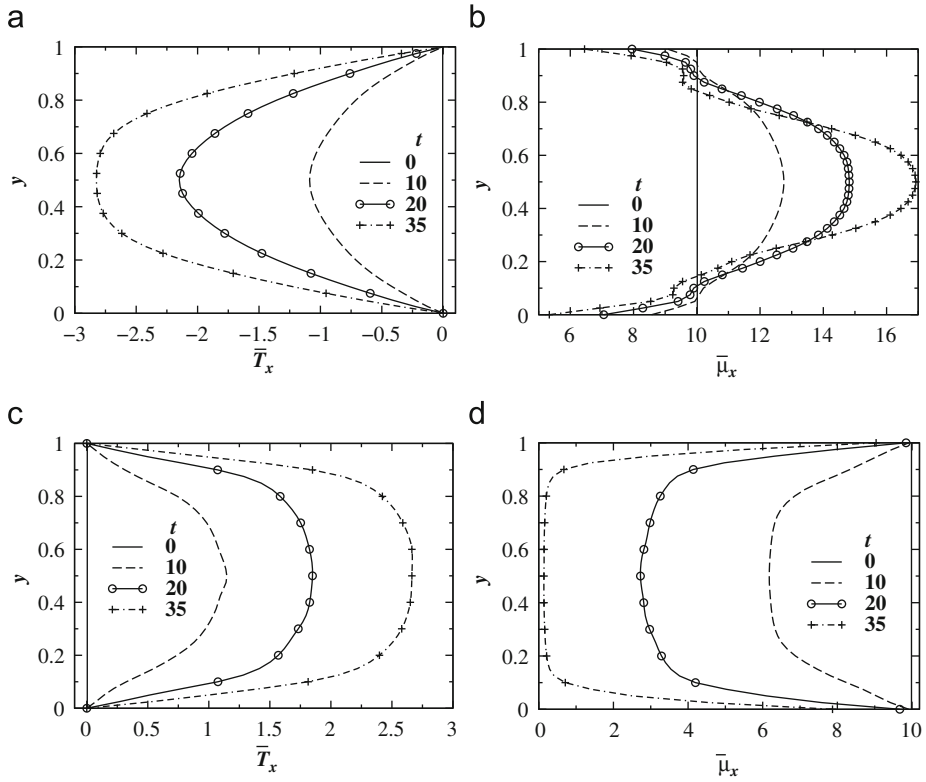

Fig. 6. Evolution of the transverse variation of the axial-averaged temperature ($\overline{T}_x \equiv (1/L)\int_0^L T\,dx$) and viscosity ($\overline{\mu}_x \equiv (1/L)\int_0^L \mu\,dx$) for $r_T = -3$ and $r_T = 3$ are shown in (a) and (b), and (c) and (d), respectively. The rest of the parameter values remain unchanged from those used to generate Fig. 3.

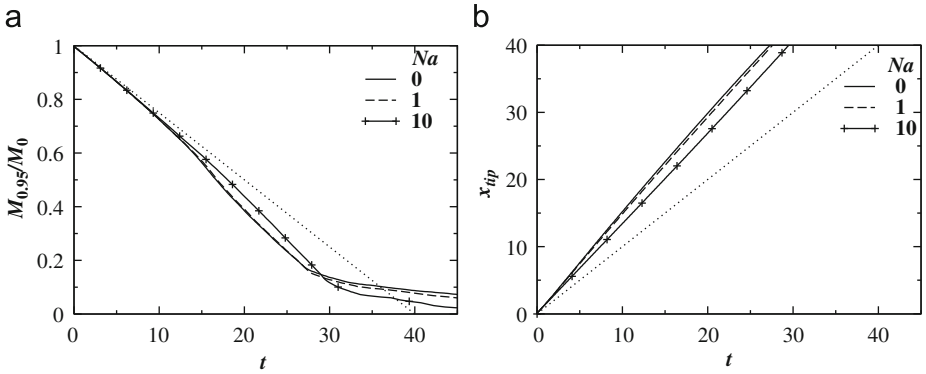

Fig. 7. The effect of *Na* on the mass fraction of the displaced fluid '1', (a), the temporal evolution of the position of the leading 'front' separating the two fluids x_{tip}, (b). The rest of the parameter values are $Re = 500$, $Sc = 100$, $Pr = 7$, $m = 10$, $r_\kappa = 1$ and $r_T = 1$. The dotted line in panel (a) is the analogue of those shown in Figs. 2a and 4a; and the dotted line in panel (b) is the analogue of those shown in Figs. 2b and 4b.

following the passage of the 'finger' (after $t \approx 30$ for $Na = 10$) increases with *Na*, as shown in Fig. 7a.

4. Concluding remarks

We have studied the nonlinear dynamics of the non-isothermal, pressure-driven displacement of one fluid by another in horizontal channels in the presence of viscous heating. We have solved numerically the continuity, Navier–Stokes and energy conservation equations coupled by a viscosity that depends on the concentration of the more viscous fluid as well as the temperature. The concentration is governed by a convective-diffusion equation. The governing equations are rendered dimensionless and are parameterized by Reynolds and Schmidt numbers in addition to a non-dimensional temperature of the invading fluid, and a Nahme number that characterizes the level of viscous heating. The results of our transient simulations have demonstrated the development of instabilities, which are driven by viscosity contrasts, that manifest themselves via the formation of vortical structures and 'roll-up' of the 'interface' that lead to fluid mixing; the intensity of mixing increases with increasing temperature of the displacing fluid leading to faster displacement of the fluid originally occupying the channel. With increasing Nahme number, we have found that high levels of viscous heating give rise to high temperatures in the regions adjacent to channel walls with correspondingly lower viscosity than in the channel core. This then leads to a situation where a high-viscosity fluid moves through the channel with the low-viscosity wall regions providing 'lubrication'. This acts to retard the propagation of the invading fluid through the channel but accelerates the ultimate displacement of the resident fluid.

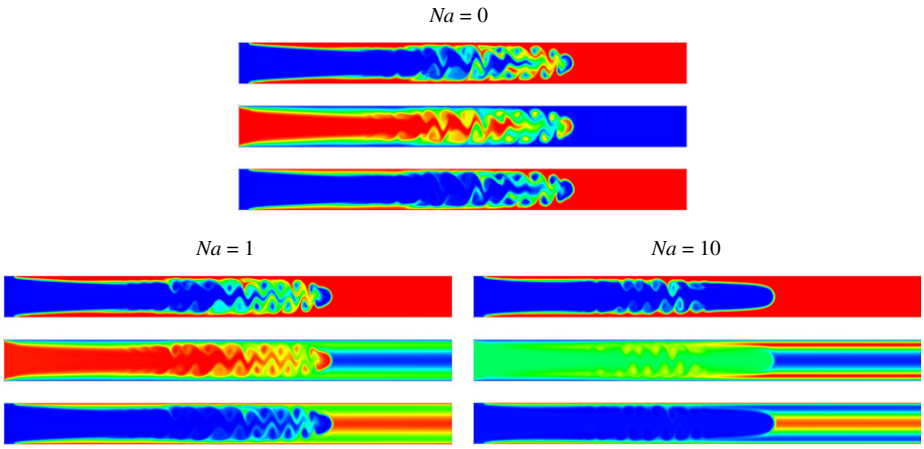

Fig. 8. The concentration, temperature and viscosity contours at t=20 for different Na are shown in first, second and third panels, respectively. The rest of the parameter values remain unchanged from those used to generate Fig. 7.

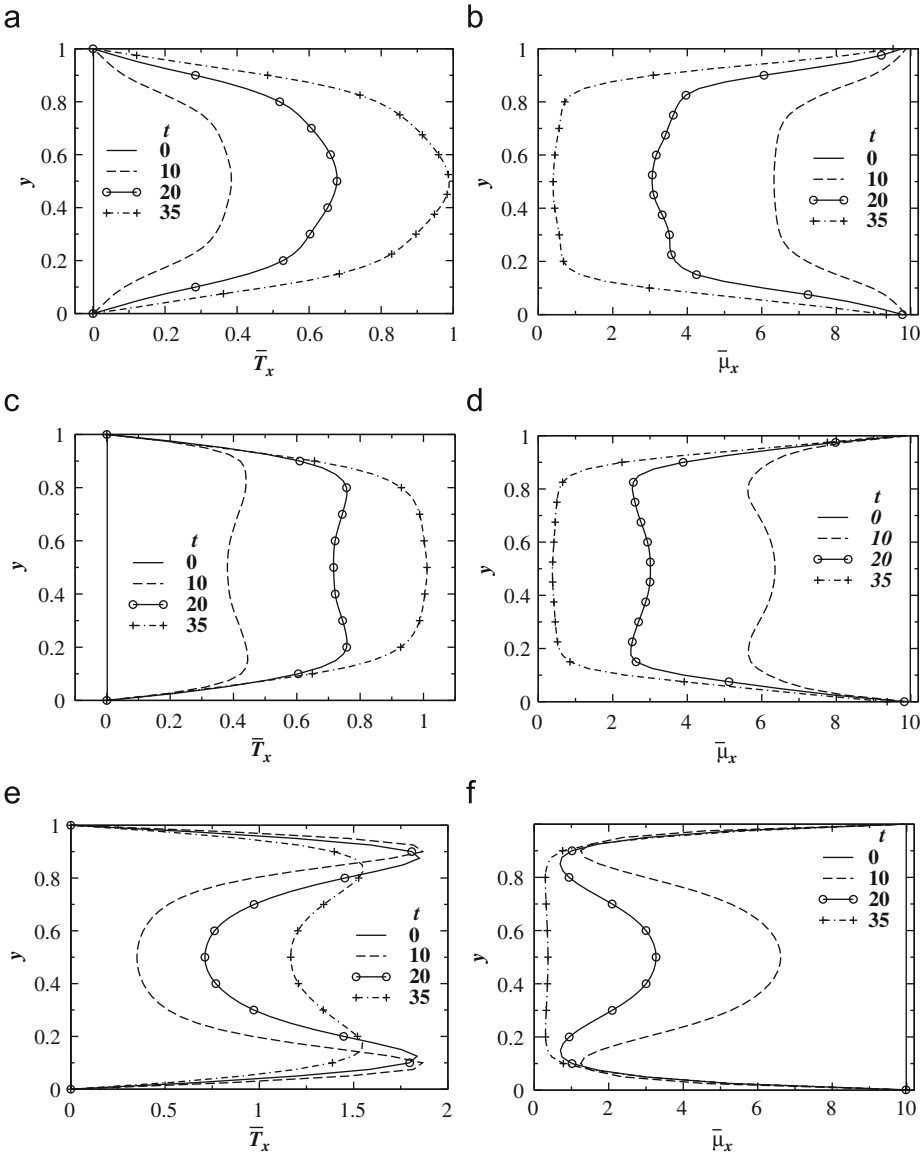

Fig. 9. Evolution of the transverse variation of the axial-averaged temperature ($\bar{T}_x \equiv (1/L)\int_0^L T\,dx$) and viscosity ($\bar{\mu}_x \equiv (1/L)\int_0^L \mu\,dx$) for Na=0, 1 and 10 are shown in (a) and (b), and (c) and (d), and (e) and (f), respectively. The rest of the parameter values remain unchanged from those used to generate Fig. 7.

Acknowledgements

We thank the Engineering and Physical Sciences Research Council UK (through Grant nos. EP/E046029/1 and EP/D503051) and the Technology Strategy Board UK (through Grant no. TP//ZEE/6/1/21191) for their support.

References

Bai, R., Chen, K., Jospeh, D.D., 1992. Lubricated pipelining: stability of core annular flow. Part 5. Experiments and comparison with theory. J. Fluid Mech. 240, 97.
Balasubramaniam, R., Rashidnia, N., Maxworthy, T., Kuang, J., 2005. Instability of miscible interfaces in a cylindrical tube. Phys. Fluids 17, 052103.
Boomkamp, P.A.M., Miesen, R.H.M., 1996. Classification of instabilities in parallel two-phase flow. Int. J. Multiphase Flow 22, 67.
Cao, Q., Ventresca, L., Sreenivas, K.R., Prasad, A.K., 2003. Instability due to viscosity stratification downstream of a centreline injector. Can. J. Chem. Eng. 81, 913.
Charles, M.E., Govier, G.W., Hodgson, G.W., 1961. The horizontal pipeline flow of equal density oil-water mixtures. Can. J. Chem. Eng. 39, 27–36.
Chen, C.Y., Meiburg, E., 1996. Miscible displacement in capillary tubes. Part 2. Numerical simulations. J. Fluid Mech. 326, 57.
Chomaz, J.-M., 2005. Global instabilities in spatially developing flows: non-normality and nonlinearity. Ann. Rev. Fluid Mech. 37, 357–392.
Cox, B.G., 1962. On driving a viscous fluid out of a tube. J. Fluid Mech. 14, 81.
Ding, H., Spelt, P.D.M., Shu, C., 2007. Diffuse interface model for incompressible two-phase flows with large density ratios. J. Comput. Phys. 226, 2078–2095.
d'Olce, M., Martin, J., Rakotomalala, N., Salin, D., Talon, L., 2008. Pearl and mushroom instability patterns in two miscible fluids' core annular flows. Phys. Fluids 20, 024104.
d'Olce, M., Martin, J., Rakotonalala, N., Salin, D., Talon, L., 2009. Convective/absolute instability in miscible core-annular flow. Part 1: experiments. J. Fluid Mech. 618, 305.
Ern, P., Charru, F., Luchini, P., 2003. Stability analysis of a shear flow with strongly stratified viscosity. J. Fluid Mech. 496, 295.
Gabard, C., Hulin, J.-P., 2003. Miscible displacement of non-newtonian fluids in a verticl tube. Eur. Phys. J. E 11, 231.
Govindarajan, R., 2004. Effect of miscibility on the linear instability of two-fluid channel flow. Int. J. Multiphase Flow 30, 1177–1192.
Hickox, C.E., 1971. Instability due to viscosity and density stratification in axisymmetric pipe flow. Phys. Fluids 14, 251.
Hinch, E.J., 1984. A note on the mechanism of the instability at the interface between two shearing fluids. J. Fluid Mech. 144, 463.
Hooper, A.P., Boyd, W.G.C., 1983. Shear flow instability at the interface between two fluids. J. Fluid Mech. 128, 507.
Hu, H.H., Joseph, D.D., 1989. Lubricated pipelining: stability of core-annular flows. Part 2. J. Fluid Mech. 205, 395.
Hu, H.H., Lundgren, T.S., Joseph, D.D., 1990. Stability of core-annular flow with a small viscosity ratio. Phys. Fluids A 2, 1945.
Hu, H.H., Patankar, N., 1995. Non-axisymmetric instability of core-annular flow. J. Fluid Mech. 290, 213.
Huerre, P., Monkewitz, P.A., 1990. Local and global instability in spatially developing flows. Ann. Rev. Fluid Mech. 22, 473–537.
Joseph, D.D., Bai, R., Chen, K.P., Renardy, Y.Y., 1997. Core-annular flows. Ann. Rev. Fluid Mech. 29, 65.
Joseph, D.D., Renardy, M., Renardy, Y.Y., 1984. Instability of the flow of two immiscible liquids with different viscosities in a pipe. J. Fluid Mech. 141, 309.
Joseph, D.D., Renardy, Y.Y., 1992. Fundamentals of Two-Fluid Dynamics. Part I: Mathemtical Theory and Applications. Springer, New York.
Kouris, C., Tsamopoulos, J., 2001a. Core-annular flow in a periodically constricted circular tube. Part 1. Steady-state linear stability and energy analysis. J. Fluid Mech. 432, 31.
Kouris, C., Tsamopoulos, J., 2001b. Dynamics of axisymmetric core-annular flow in a straight tube. I. The more viscous fluid in the core, bamboo waves. Phys. Fluids 13, 841.
Kouris, C., Tsamopoulos, J., 2002a. Core-annular flow in a periodically constricted circular tube. Part 2. Nonlinear dynamics. J. Fluid Mech. 470, 181.
Kouris, C., Tsamopoulos, J., 2002b. Dynamics of axisymmetric core-annular flow in a straight tube. II. The less viscous fluid in the core, saw tooth waves. Phys. Fluids 14, 1011.
Kuang, J., Maxworthy, T., Petitjeans, P., 2003. Miscible displacements between silicone oils in capillary tubes. Eur. J. Mech. 22, 271.
Lajeunesse, E., Martin, J., Rakotomalala, N., Salin, D., 1997. 3d instability of miscible displacements in a hele-shaw cell. Phys. Rev. Lett. 79, 5254.
Lajeunesse, E., Martin, J., Rakotomalala, N., Salin, D., Yortsos, Y.C., 1999. Miscible displacement in a Hele–Shaw cell at high rates. J. Fluid Mech. 398, 299.
Li, J., Renardy, Y.Y., 1999. Direct simulation of unsteady axisymmetric core-annular flow with high viscosity ratio. J. Fluid Mech. 391, 123.
Malik, S.V., Hooper, A.P., 2005. Linear stability and energy growth of viscosity stratified flows. Phys. Fluids 17, 024101.
Nahme, R., 1940. Beiträge zur hydrodynamischen theorie der lagerreibung. Ingenieur-Archiv 11, 191–209.
Petitjeans, P., Maxworthy, T., 1996. Miscible displacements in capillary tubes. Part 1. Experiments. J. Fluid Mech. 326, 37.
Pinarbasi, A., Ozalp, C., 2001. Effect of viscosity models on the stability of a non-Newtonian fluid in a channel with heat transfer. Int. Commun. Heat Mass Transf. 28 (3), 369–378.
Preziosi, L., Chen, K., Joseph, D.D., 1989. Lubricated pipelining: stability of core-annular flow. J. Fluid Mech. 201, 323.
Ranganathan, B.T., Govindarajan, R., 2001. Stabilisation and destabilisation of channel flow by location of viscosity-stratified fluid layer. Phys. Fluids 13 (1), 1–3.
Regner, M., Henningsson, M., Wiklund, J., Östergren, K., Trägårdh, C., 2007. Predicting the displacement of yoghurt by water in a pipe using cfd. Chem. Eng. Technol. 30, 844–853.
Renardy, Y.Y., Joseph, D.D., 1985. Couette-flow of two fluids between concentric cylinders. J. Fluid Mech. 150, 381–394.
Sahu, K.C., Ding, H., Valluri, P., Matar, O.K., 2009a. Linear stability analysis and numerical simulation of miscible channel flows. Phys. Fluids 21, 042104.
Sahu, K.C., Ding, H., Valluri, P., Matar, O.K., 2009b. Prssure-driven miscible two-fluid channel flow with density gradients. Phys. Fluids 21, 043603.
Sahu, K.C., Matar, O.K., 2010. Stability of plane channel flow with viscous heating. J. Fluids Eng. 132, 011202.
Schmid, P.J., Henningson, D.S., 2001. Stability and Transition in Shear Flows. Springer, New York.
Scoffoni, J., Lajeunesse, E., Homsy, G.M., 2001. Interface instabilities during displacement of two miscible fluids in a vertical pipe. Phys. Fluids 13, 553.
Selvam, B., Merk, S., Govindarajan, R., Meiburg, E., 2007. Stability of miscible core-annular flows with viscosity stratification. J. Fluid Mech. 592, 23–49.
Selvam, B., Merk, S., Govindarajan, R., Meiburg, E., 2009. Convective/absolute instability in miscible core-annular flow. Part 2. Numerical simulations and nonlinear global modes. J. Fluid Mech. 618, 323.
Sukanek, P.C., Goldstein, C.A., Laurence, R.L., 1973. The stability of plane channel flow with viscous heating. J. Fluid Mech. 57, 651–670.
Taylor, G.I., 1961. Deposition of viscous fluid on the wall of a tube. J. Fluid Mech. 10, 161.
Wei, H.H., Rumschitzki, D.S., 2002a. The linear stability of a core-annular flow in an asymptotically corrugated tube. J. Fluid Mech. 466, 113.
Wei, H.H., Rumschitzki, D.S., 2002b. The weakly nonlinear interfacial stability of a core-annular flow in a corrugated tube. J. Fluid Mech. 466, 149.
Yiantsios, S.G., Higgins, B.G., 1988. Numerial solution of eigenvalue problems using the compound matrix-method. J. Comput. Phys. 74, 25.
Yih, C.S., 1967. Instability due to viscous stratification. J. Fluid Mech. 27, 337.